Electronic Supplementary Information

For

Low Temperature Synthesized Ultrathin γ-Fe_2O_3 Nanosheets Show Similar Adsorption Behavior for As(III) and As(V)

Rui Liu,[a] *Jing-Fu Liu,*[*, a,b] *Li-Qiang Zhang,*[c] *Jie-Fang Sun,*[a] *and Gui-Bin Jiang*[a]

[a] State Key Laboratory of Environmental Chemistry and Ecotoxicology, Research Center for Eco-Environmental Sciences, Chinese Academy of Sciences, Beijing 100085, China.

[b] Institute of Environment and Health, Jianghan University, Hubei Province, Wuhan 430056, China

[c] State Key Laboratory of Heavy Oil Processing and Department of Materials Science and Engineering, China University of Petroleum, Beijing 102249, China

E-mail: jfliu@rcees.ac.cn

S1.Experiment Section

S 1.1 Materials and Chemicals.

Triton X-114 (TX-114) was purchased from Acros Organics (Geel, Belgium). $NaAsO_2$, $Na_2HAsO_4 \cdot 7H_2O$, $FeCl_3$, Na_3PO_4, NaCl, HNO_3, and KOH were supplied by Sinopharm Chemical Reagent Co. (Beijing, China). KBH_4 was purchased from Jinke Chemical Research Institute (Tianjin, China). All the chemicals were of at least analytic grade. Ultrapure water (Millipore, Bedford, MA) was used throughout this study.

S 1.2 Characterizations

The crystal structure was determined by X-ray diffraction (XRD) analysis, which was performed with an X' pert PRO instrument (PANalytical) using Cu Kα radiation (λ = 0.15418 nm). The chemical state was probed by X-ray photoelectron spectroscopy (XPS) analysis on AXIS ULTRADLD. For XRD analysis, samples were freeze-dried at -55 ^oC in high vacuum, the resulting blank/brown powder was place on Si wafers with high index facet to form a thin layer. The XPS samples were prepared by the same method for XRD analysis, but the separated black slurry was dipped on Si wafer directly, freeze-dried at -55 ^oC and stored at high vacuum, and the total air exposure time was less than 1 hour to suppress O_2 induced oxidation. The morphology of NSs was observed by high resolution transmission electron microscopy (HRTEM) and field emission scanning electron microscopy (FESEM). HRTEM analysis was fulfilled on a Tecnai G2 F-20(FEI) HRTEM, the species were prepared by loading 3 μL aliquots of the aqueous sample onto ultra-thin amorphous carbon film-coated copper grid sample holders, and excess water was removed quickly with filter paper. FESEM was conducted on SU-8020 (Hitachi), the species were prepared by loading 10.0 μL aliquots of the aqueous sample onto Si wafer, after stored in 4oC for 30 min, excess water was removed quickly with filter paper. Besides HRTEM and XRD, Raman spectra was also utilized to determine the crystal structure of synthesized nanosheets, and for the enhancing the weak Raman signal, Ag nanoporous film was utilized as Raman enhancement substrate. The sample was prepared by dip 10 uL wet precipitate on Ag nanoporous film (Figure S4).[1] 532 nm laser was employed as the excitation source, the laser

power was maintained at about 50 uW at sample to suppress the photo damage/photo induced crystal structure change, the total accumulation time was 30s ×10. The FTIR measurements were performed using a Thermo-Nicolet Nexus 6700 FTIR spectrometer, samples for FTIR determination were ground with special grade KBr in an agate mortar.

S 1.3 X-ray Adsorption Spectra

The As K-edge EXAFS spectra were collected at beamline 14W1 of the Shanghai Synchrotron Radiation Facility (SSRF). The spectra were taken under standard SSRF operation conditions (2.8 GeV and 150-280 mA) with a double-crystal Si(111) monochromator. The spectra were collected in fluorescence mode using a Lytle fluorescence ion chamber detector positioned at a 90 ° angle to the incident beam at room temperature. Spectra from −200 to 1000 eV relative to the As K edge were acquired. Standard reference chemicals, $Na_2HAsO_4 \cdot 7H_2O$, $NaAsO_2$ were also analyzed. Elemental arsenic (As^0) was used to calibrate the energy at 11 868 eV.

S 1.4 EXAFS data analysis

EXAFS data analysis was performed using the ATHENA and AETEMIS program in the Demeter computer package.[2, 3] The analysis procedure was similar to our previous studies.[4, 5] The raw data measured in intensities were converted to μ(E), and averaged spectra were used in the analysis. The EXAFS signal χ(*k*) was extracted from the measured data using the AUTOBK algorithm where *k* is the photoelectron wave number.[6] The primary quantity for EXAFS is then χ(*k*), the oscillations as a function of photoelectron wave number. χ(*k*) was weighted by k^2 to account for the dampening of oscillations with increasing *k*. The different frequencies in the oscillations in χ(k) correspond to different near neighbor coordination shells which can be described and modeled according to the EXAFS equation

$$\chi(k) = \sum_j \frac{N_j f_j(k) e^{-2k^2\sigma_j^2}}{kR_j^2} \sin[2kR_j + \delta_j(k)]$$

where f(*k*) and δ(*k*) represent the photoelectron backscattering amplitude and phase shift, respectively, N is the number of neighboring atoms, R is the distance to the neighboring atom, and the σ^2 is the Debye-Waller factor representing the disorder in the neighbor distance. The k^3

weighted EXAFS in k-space ($Å^{-1}$) was Fourier transformed (FT) to produce the radial structure function (RSF) in R-space (Å). The experimental spectra were fitted with single-scattering theoretical phase-shift and amplitude functions calculated with the *ab initio* computer code FEFF6 using atomic clusters generated from the crystal structure of $FeAsO_4$.[7] The many-body amplitude reduction factor (S_0^2) was established as 0.95 by isolating and fitting the first-shell As-O of the spectrum. The spectrum was fit by first isolating and fitting the first-shell As-O to estimate ΔE_0, the difference in threshold energy between theory and experiment. Then ΔE_0 was fixed to the best fit value from first-shell fitting and kept the same for all interatomic shells in a given spectrum. In addition, the ΔE0 value was allowed to float by no more than ±10 eV. The parameters such as interatomic distance (R), coordination number (CN), and Debye-Waller factor (σ^2) were first established with reasonable guesses and were fitted in R-space. The error in the overall fits was determined using R-factor, the goodness-of-fit parameter: R-factor = $\Sigma(\chi_{data} - \chi_{fit})^2/\Sigma(\chi_{data})^2$. Good fits occur for R-factor < 0.05.

3. Reference

1. Liu, R.; Sun, J. F.; Cao, D.; Zhang, L. Q.; Liu, J. F.; Jiang, G. B., Fabrication of highly-specific SERS substrates by co-precipitation of functional nanomaterials during the self-sedimentation of silver nanowires into a nanoporous film. *Chem Commun* **2015,** *51*, (7), 1309-1312.
2. Newville, M., IFEFFIT: interactive XAFS analysis and FEFF fitting. *Journal of Synchrotron Radiation* **2001,** *8*, 322-324.
3. Ravel, B.; Newville, M., ATHENA, ARTEMIS, HEPHAESTUS: data analysis for X-ray absorption spectroscopy using IFEFFIT. *Journal of Synchrotron Radiation* **2005,** *12*, 537-541.
4. Jing, C. Y.; Liu, S. Q.; Patel, M.; Meng, X. G., Arsenic leachability in water treatment adsorbents. *Environ Sci Technol* **2005,** *39*, (14), 5481-5487.
5. Shi, Q. T.; Huang, Y. Y.; Jing, C. Y., Synthesis, characterization and application of lanthanum-impregnated activated alumina for F removal. *J Mater Chem A* **2013,** *1*, (41), 12797-12803.
6. Newville, M.; Livins, P.; Yacoby, Y.; Rehr, J. J.; Stern, E. A., Near-Edge X-Ray-Absorption Fine-Structure of Pb - a Comparison of Theory and Experiment. *Physical Review B* **1993,** *47*, (21), 14126-14131.
7. Deleon, J. M.; Rehr, J. J.; Zabinsky, S. I.; Albers, R. C., Abinitio Curved-Wave X-Ray-Absorption Fine-Structure. *Physical Review B* **1991,** *44*, (9), 4146-4156.
8. Cao, C. Y.; Qu, J.; Yan, W. S.; Zhu, J. F.; Wu, Z. Y.; Song, W. G., Low-Cost Synthesis of Flowerlike alpha-Fe2O3 Nanostructures for Heavy Metal Ion Removal: Adsorption Property and Mechanism. *Langmuir* **2012,** *28*, (9), 4573-4579.
9. Shi, Q. T.; Yan, L.; Chan, T. S.; Jing, C. Y., Arsenic Adsorption on Lanthanum-Impregnated

Activated Alumina: Spectroscopic and DFT Study. *Acs Appl Mater Inter* **2015,** *7*, (48), 26735-26741.

2. Figures and Tables

Figure S1. a)TEM, b) HRTEM and c), d) STEM images of γ-Fe_2O_3 NSs, all of which indicate the ultrathin characteristic of the as-synthesized nanostruture.

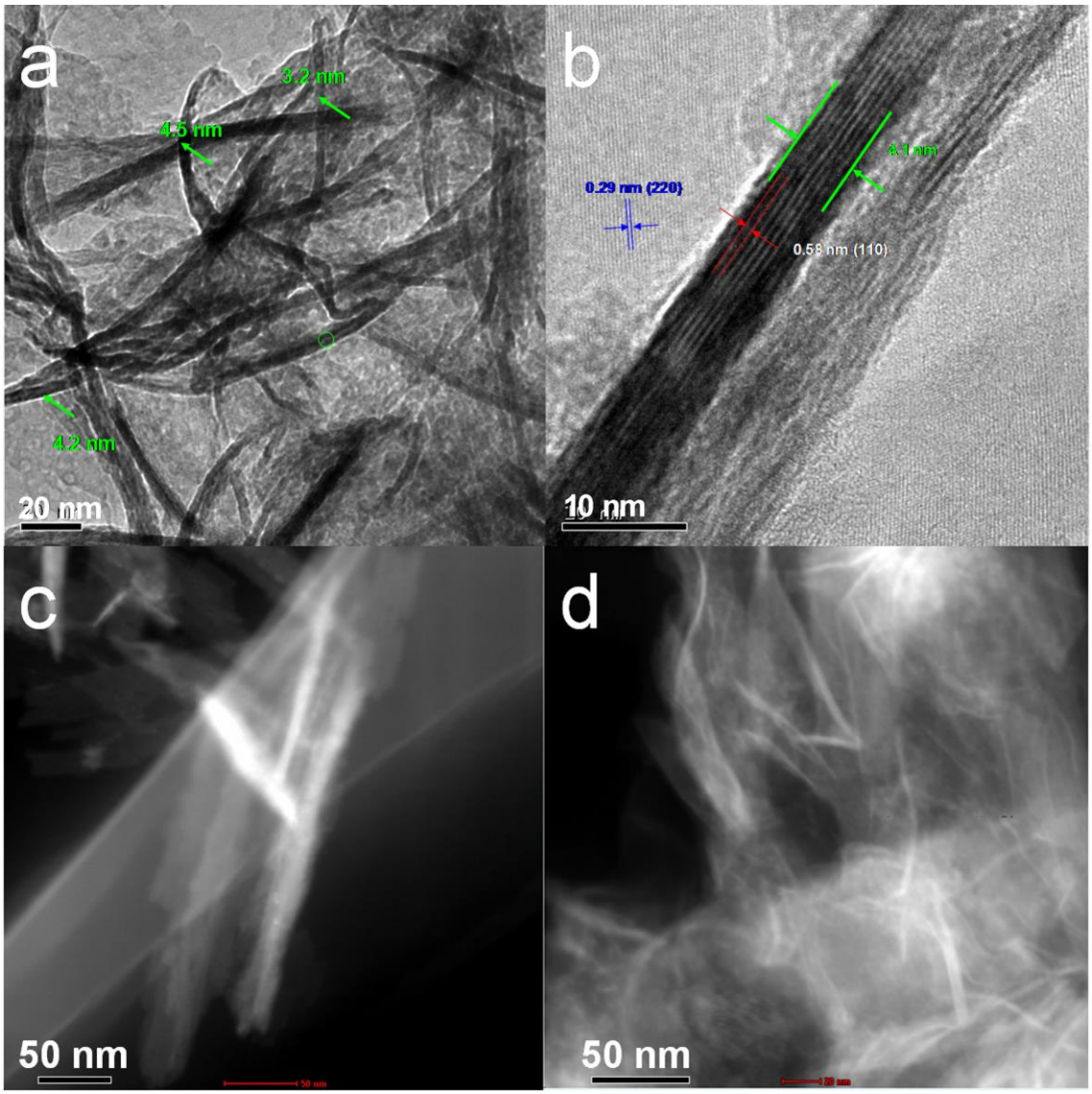

Figure S2. FESEM images of γ-Fe_2O_3 NSs.

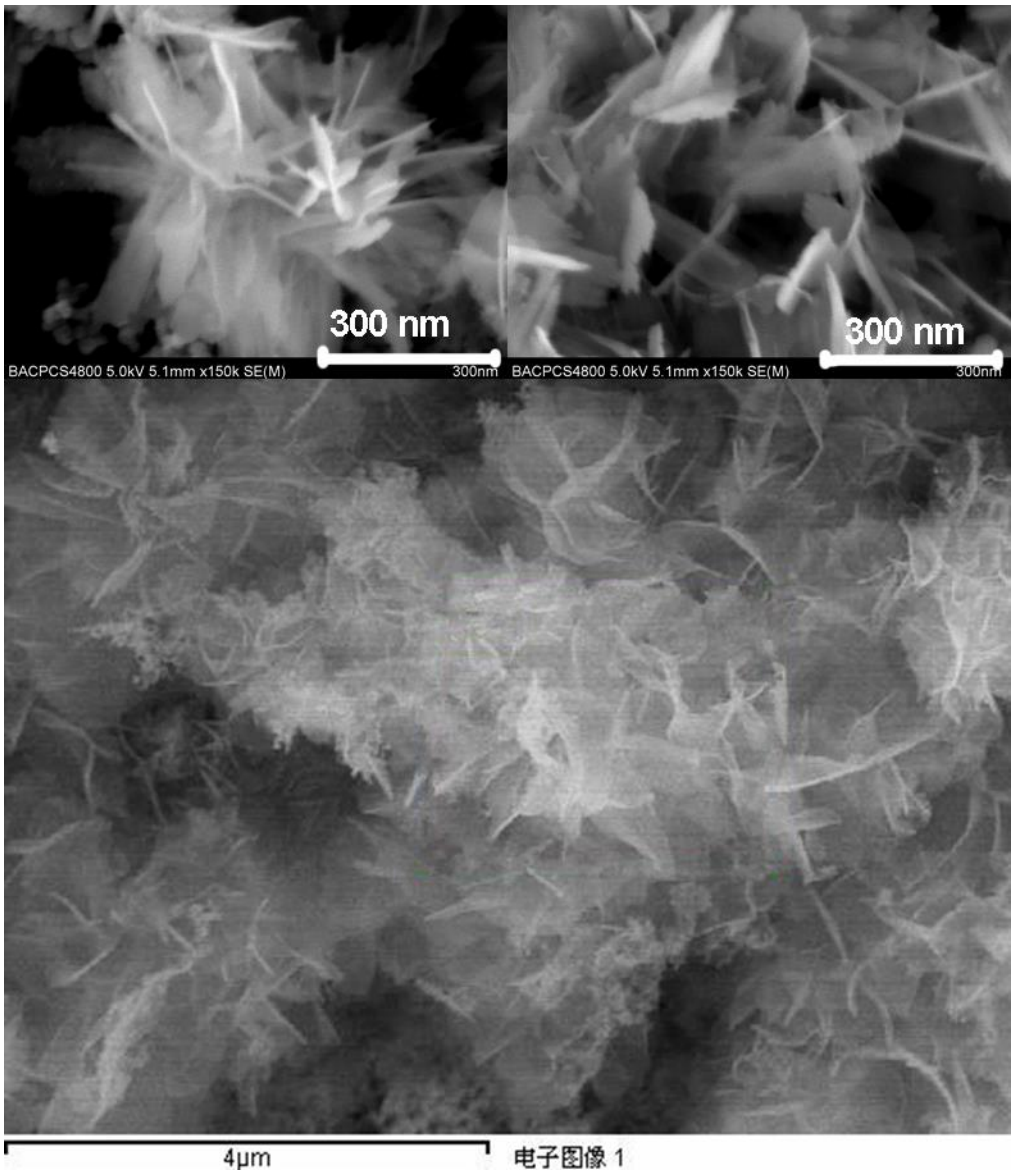

Figure S3. High-resolution Fe_{2p} XPS spectra of the γ-Fe_2O_3 NSs before and after loading As(III), the spectra of As(III) loaded Fe@Fe_2O_3 nanochains (NCs) and As(III) loaded α-Fe_2O_3 NPs were also presented for comparison. The small peak at 707 eV which associated with Fe(0) in γ-Fe_2O_3 NSs was completely disappeared after treated with As(III) for 2 h. For the presence of protective Fe_2O_3 shell on Fe(0) in Fe@Fe_2O_3 nanochains, the reaction between As(III) and Fe(0) is not as fast as that in γ-Fe_2O_3 NSs, and Fe(0) peak is also visible after treat with As(III) for 2 h. As this time, about 9.1 % of adsorbed As(III) was reduced into As(0). All samples were kept in frozen drier at high vacuum before XPS analysis to minimize the oxidation in air.

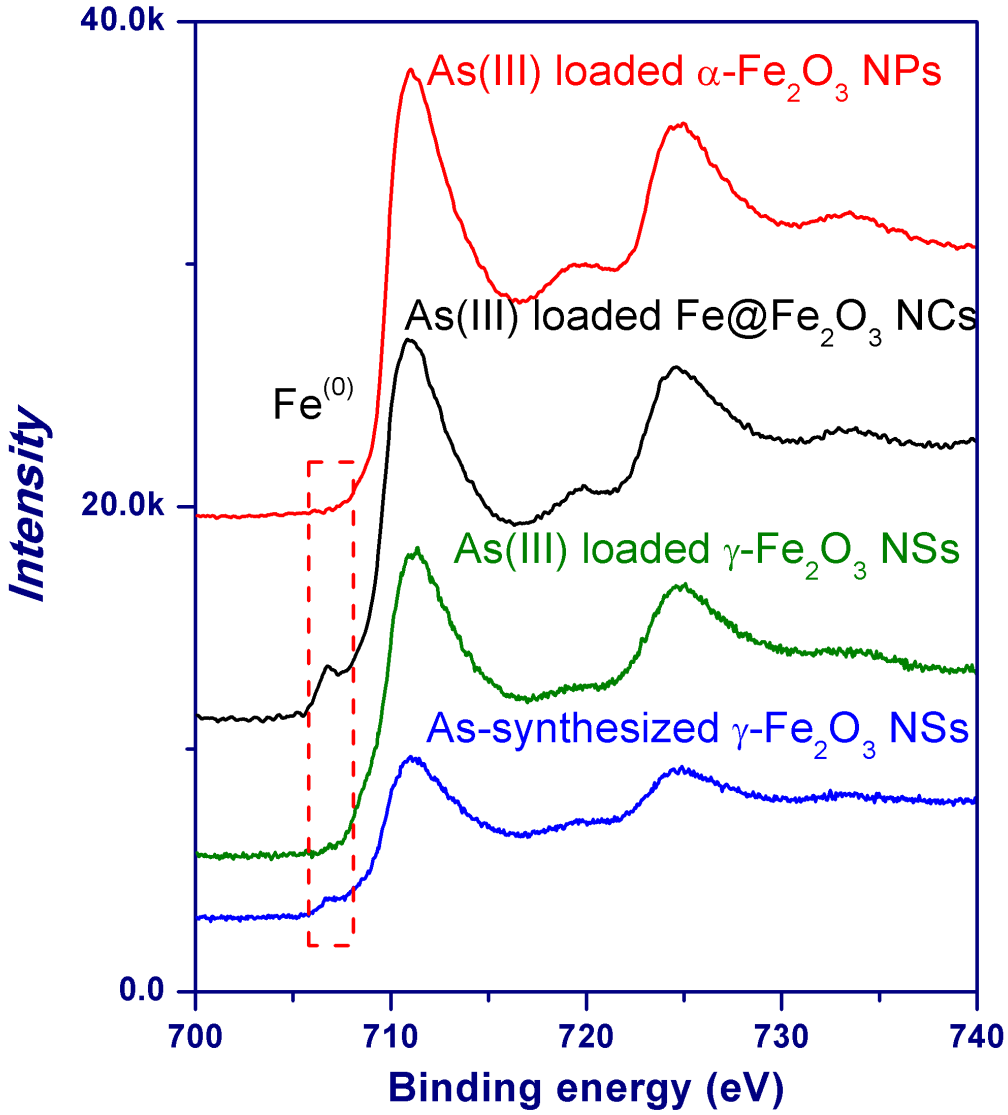

Figure S4. FESEM image of γ-Fe_2O_3 Nanosheets on Ag nanoporous film for enhanced Raman spectra collection. To acquire high quality Raman spectra of γ-Fe_2O_3 NSs at very low Laser power (50 μW, which is very crucial for the minimized sample damage or phase transform during Raman analysis), 10 μL diluted γ-Fe_2O_3 NSs water dispersion was load on Ag nanoporous film to enhance the Raman signal.

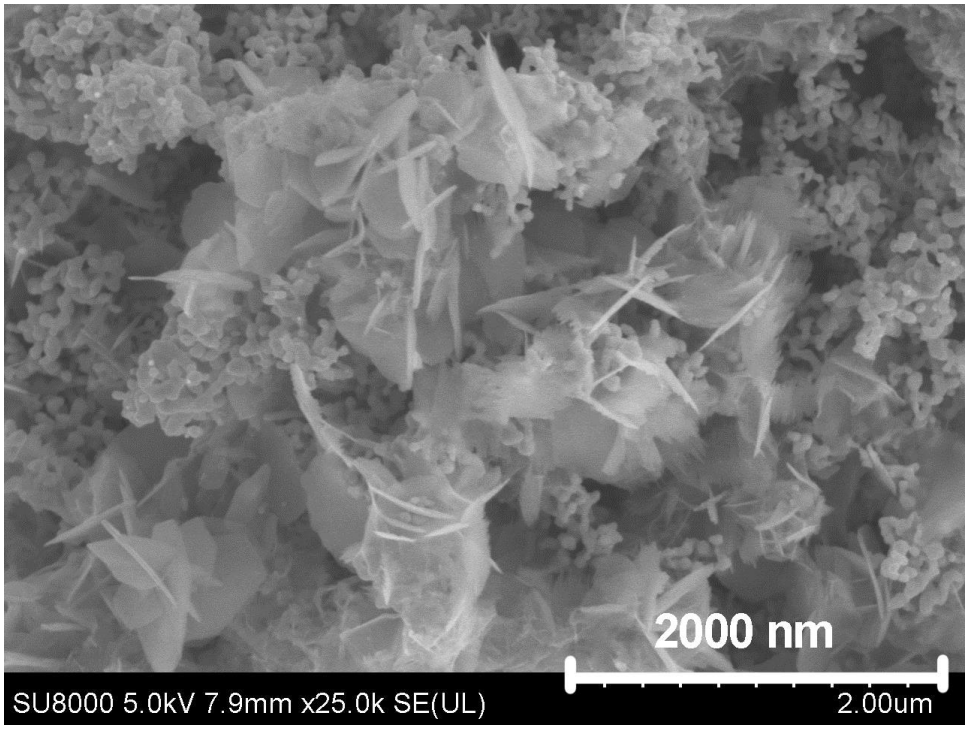

Figure S5. Room temperature hysteresis loop of fresh synthesized γ-Fe_2O_3 NSs and sample aged in air for 1 and 6 month. After aged in air for 1 month and 6 month, the room temperature saturation magnetization were reduced to 64 and 61 emu g^{-1}, respectively, which is due to the gradually oxidation Fe(0) impurity, and supports the notion that the presence of Fe(0) enhanced the magnetic response of the γ-Fe_2O_3 NSs.

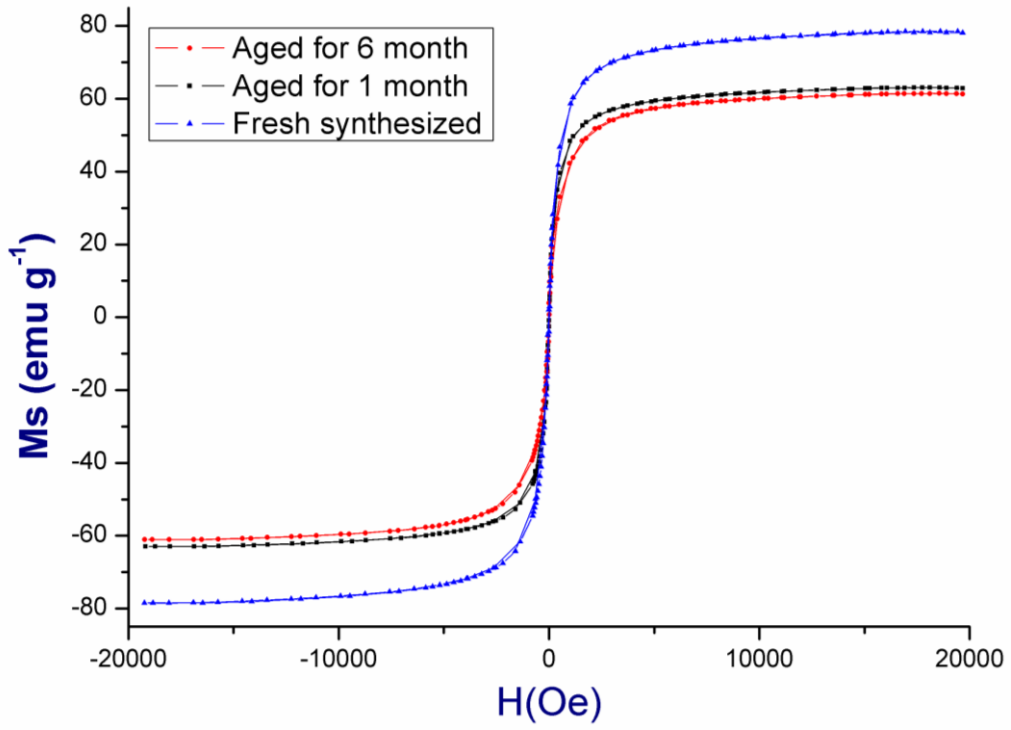

Figure S6. TEM images of synthesized nanostructure at different stage. The residue nanoclusters were highlighted by arrows. With the elongation of aging time, the amount of nanoclusters was gradually decreased, and size of NSs was kept increase with time.

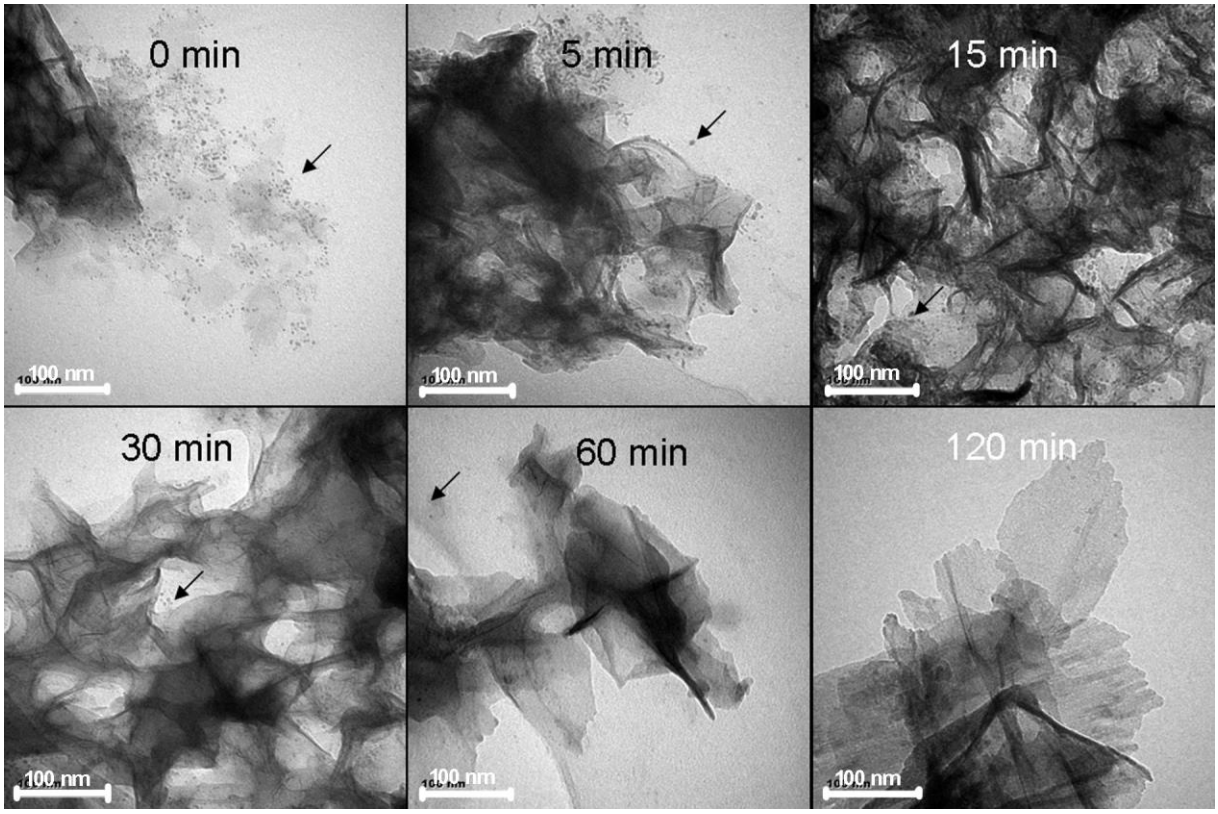

Figure S7. HRTEM images of synthesized nanostructure at different stage. Lattice analysis on all discernible area showed the Fe_3O_4 or γ-Fe_2O_3 nature of these nanoparticles. However, for the chemical instability of Fe(0) nanoclusters, the possibility of oxidizing Fe(0) on TEM grid during sample preparation and storage cannot be excluded.

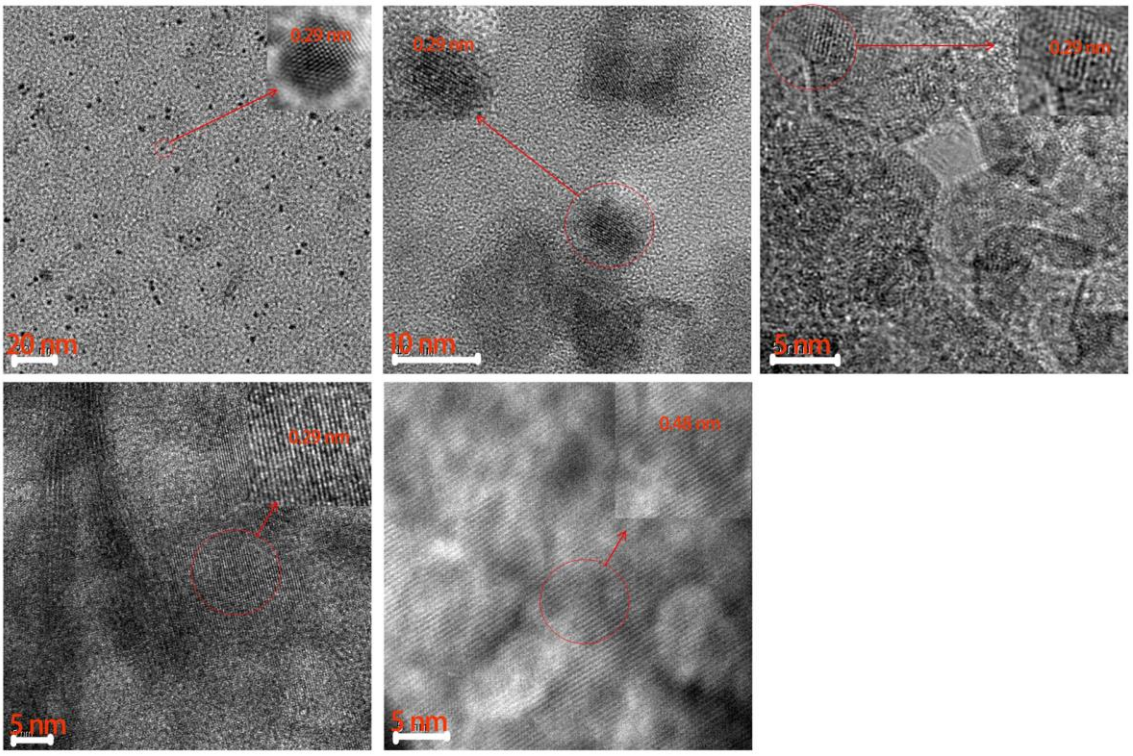

Figure S8. HRTEM images that reveals the existence of stack faults and twin boundary inside the synthesize NSs, and indirectly support the notion that the nanosheets were growth by the oriented attachment of small nanocrystal.

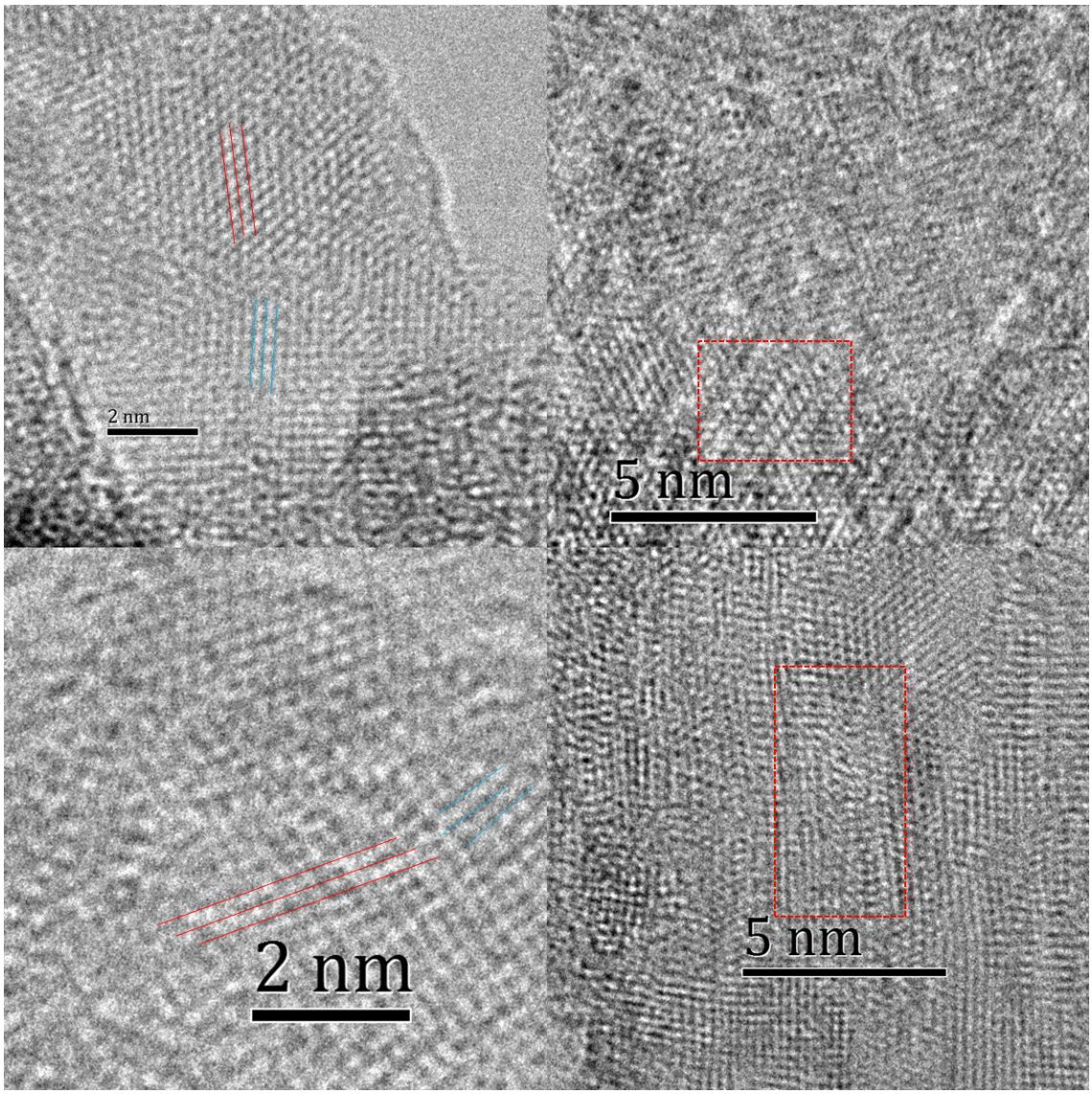

Figure S9. Effect of KBH_4 concentration on the morphology of synthesized nanostructures.

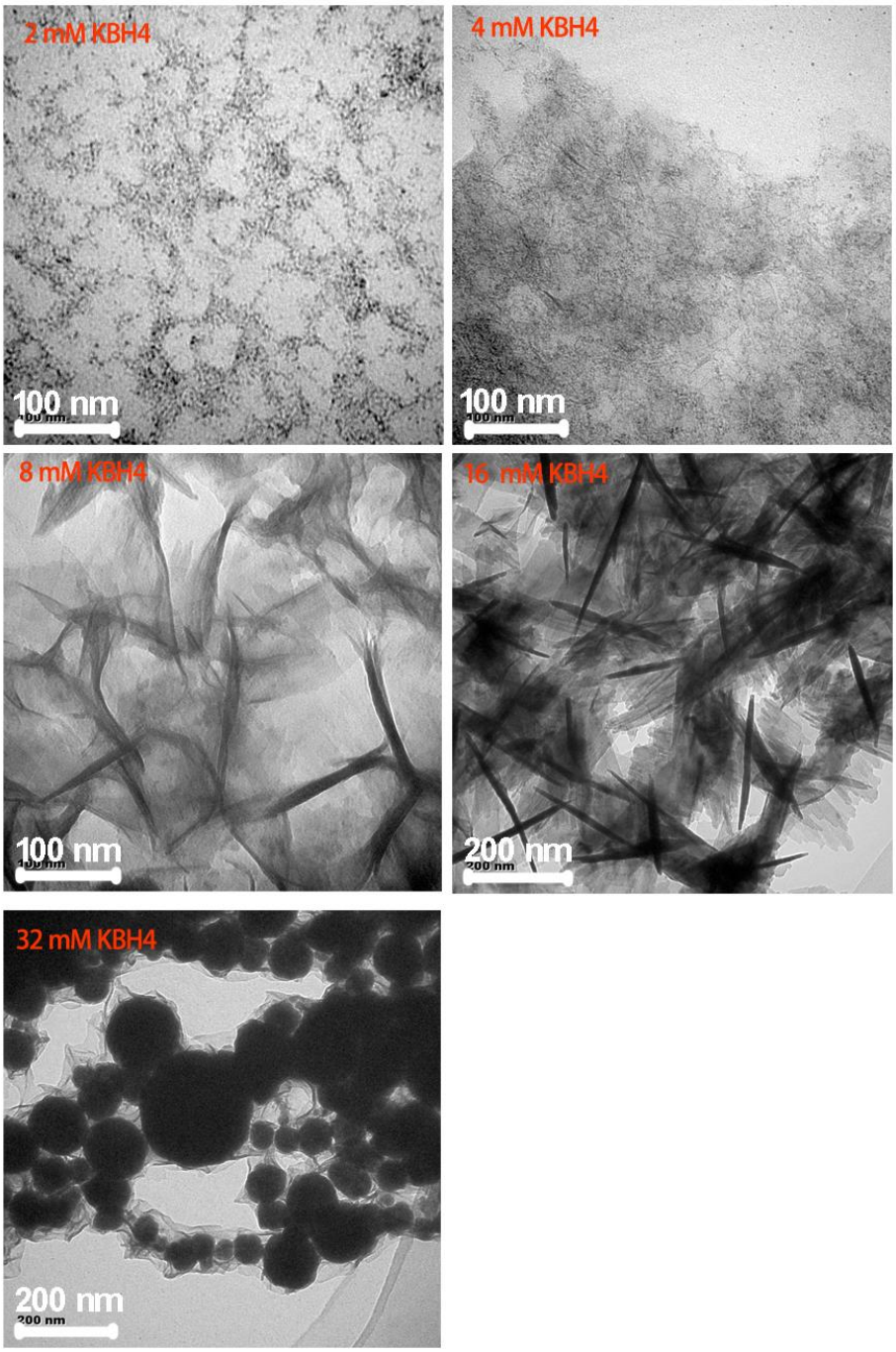

Figure S10. Effect of TX-114 concentration on the morphology of synthesized nanostructure.

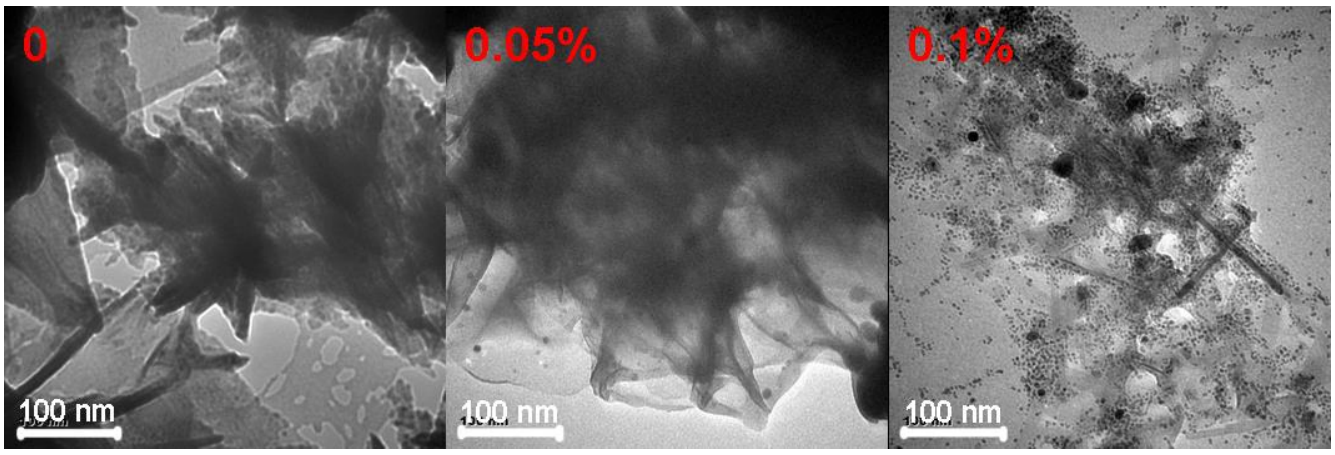

Figure S11 Summarization of the effect of reaction condition on the morphology of synthesized nanostructure and the proposed single-crystalline nanosheets growth mechanism.

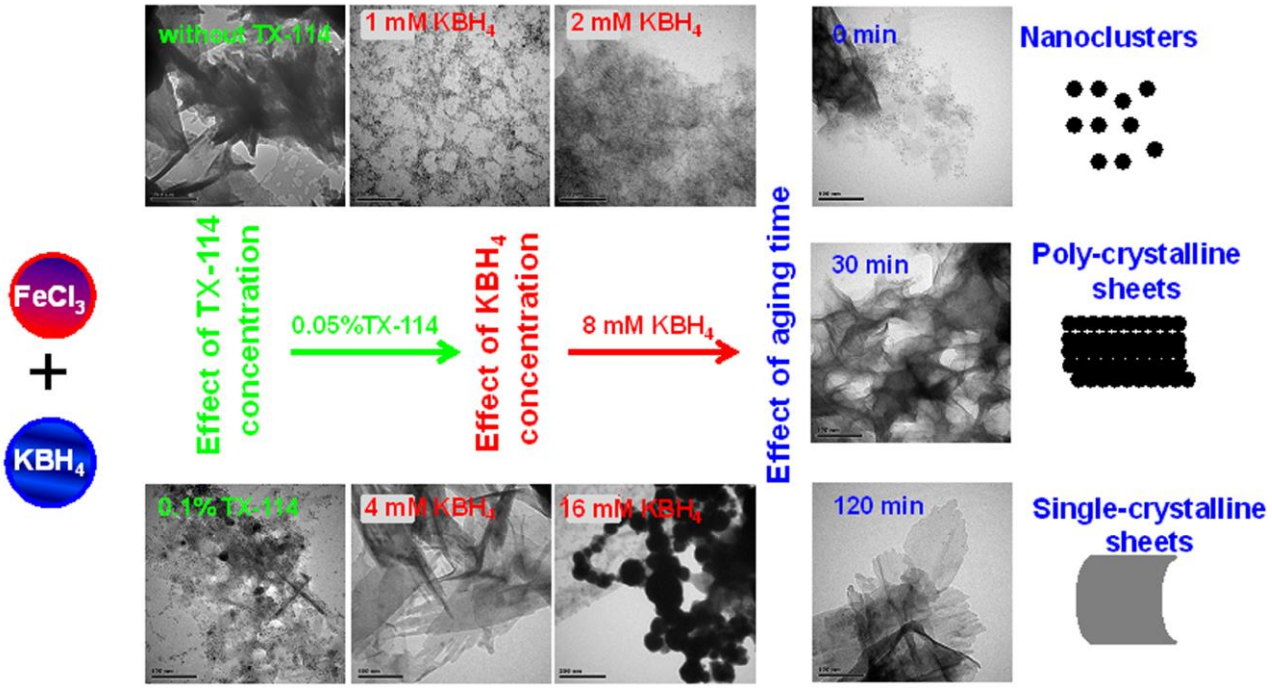

Figure S12. TEM and HRTEM images of the As(III) treated NSs (the concentration of As(III) is 10 mg L^{-1}). After treated with As(III), the NS morphology of γ-Fe_2O_3 was preserved in some extend, but some crystallized particles were also observed on the TEM grid, which may from the distroy of NS.

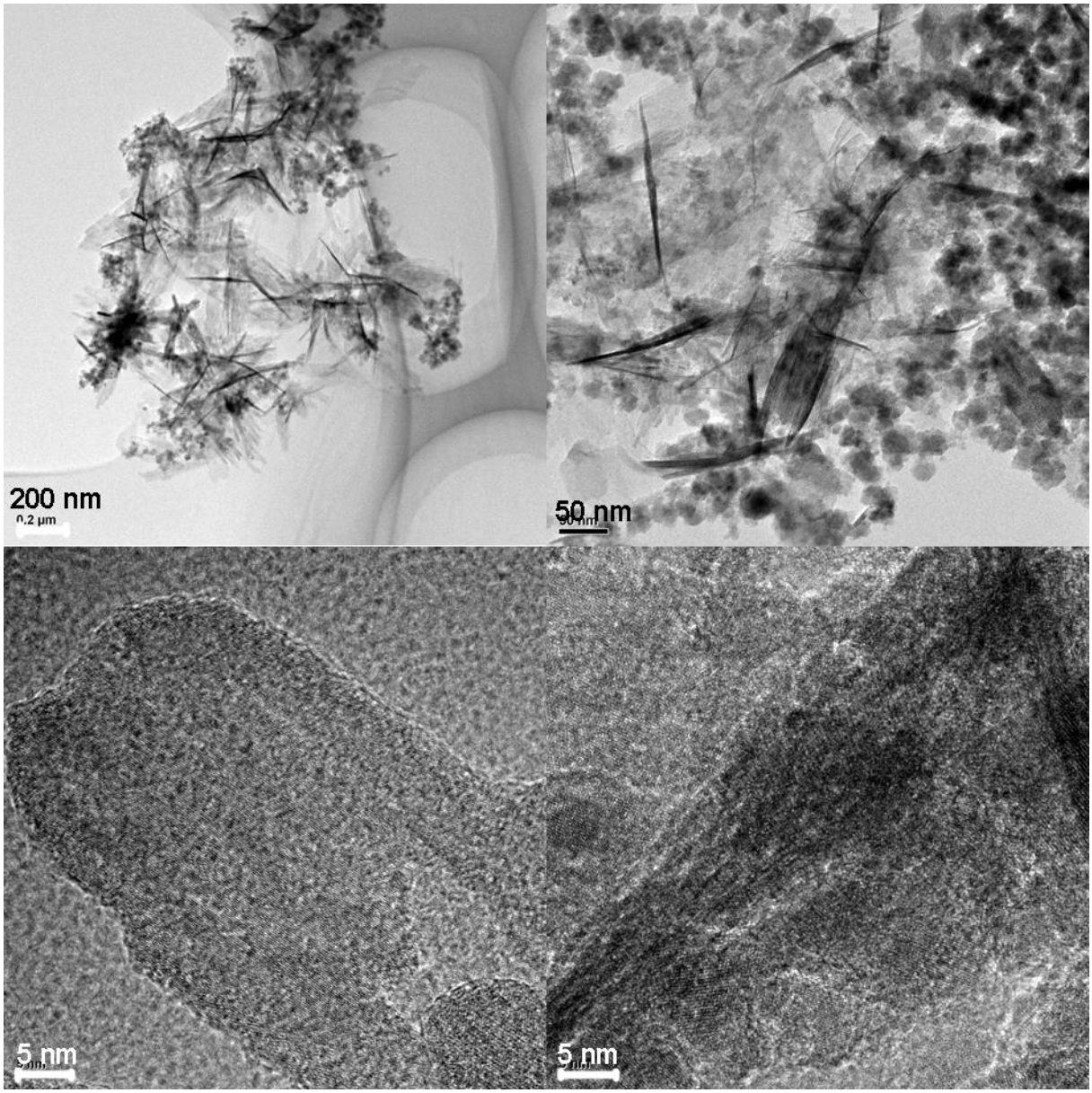

Figure S13. The FTIR spectra of the as-synthesized γ-Fe_2O_3 NSs and 10.0 mg L^{-1} As(III)/As(V) treated NSs (upper). Apparent IR band of As-O were observed at 804, 822 and 870 cm^{-1}, in constant with reported value in literature.[8, 9] The detailed IR band assignment was show in the lower graph, which is the transmittance spectrum of 10 mg L^{-1} loaded γ-Fe_2O_3 NSs. The bands of Fe-O, As-O, Fe-OH, adsorbed water, C-H, and –OH were appeared at 670, 805, 1060, 1632, 2230, 2950 and 3400 cm^{-1}, respectively.

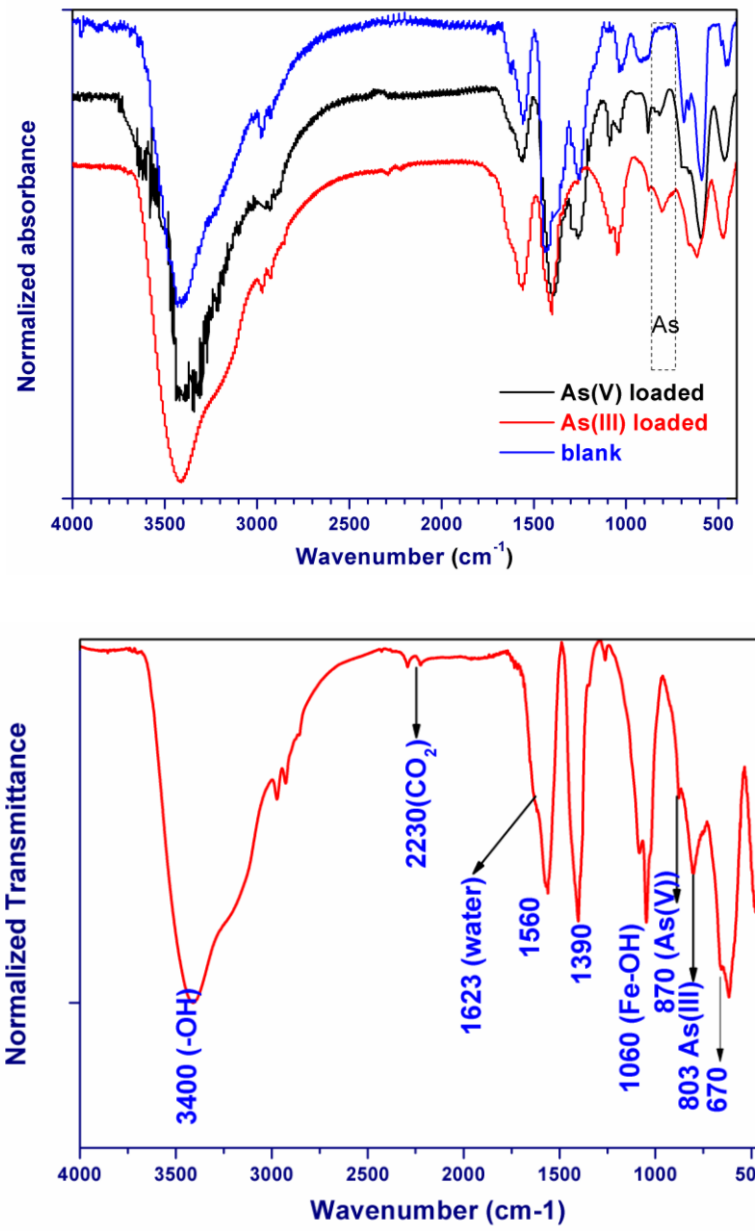

Figure S14. The removal rate of arsenic ions by 0.1 g L^{-1} γ-Fe_2O_3 NSs. For initial As(III)/As(V) with concentration no more than 2.5 mg L-1, the removal rate were higher than 95%. Higher concentration of initial As ion result in the lowered removal rate for limited adsorption sites on γ-Fe_2O_3 NSs. In all cases, the removal rate of As(III) are larger than that of As (V), again ascribed to the superior As(III) capture capacity.

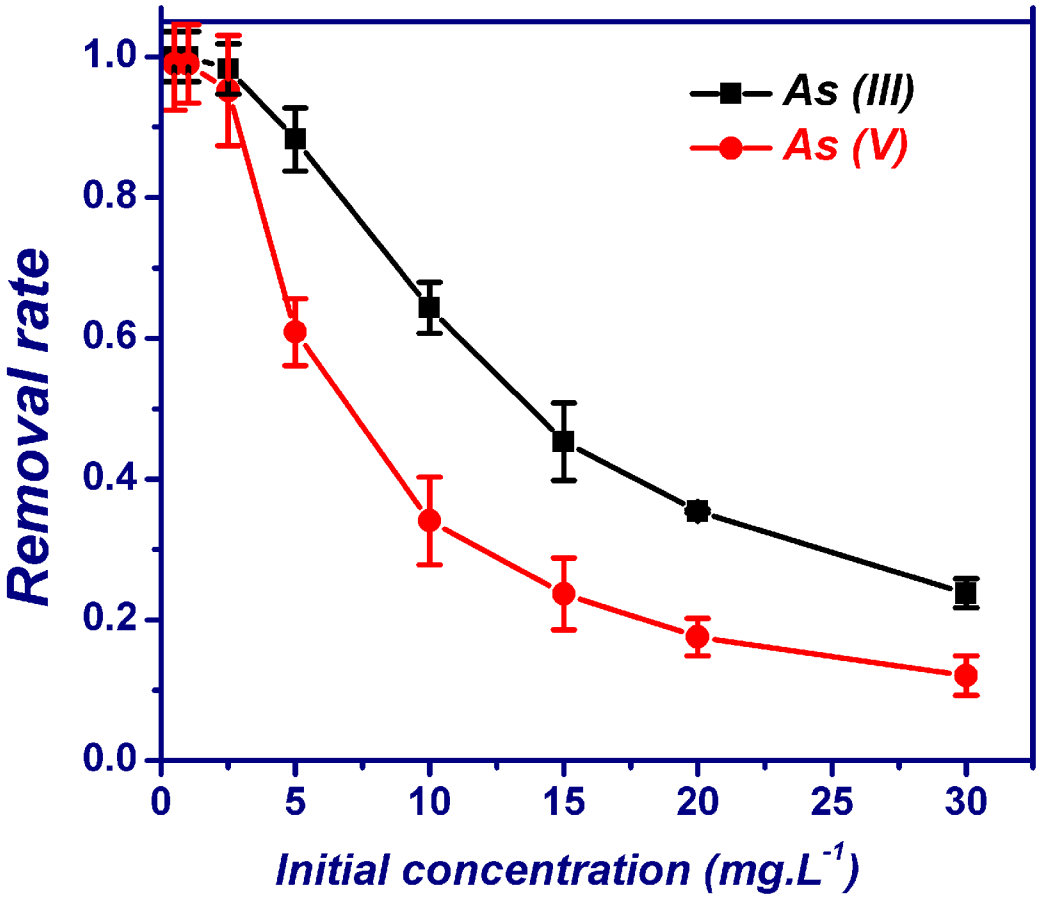

Figure S15. Deprive the adsorption capacity of NSs for As(III)/(V) by Freundlich fitting. Compared with the high linearity shown by Langmuir model, the low linearity here indicates Freundlich model is less appropriate in describing the adsorption process of Arsenic ion onγ-Fe_2O_3 NSs than Langmuir model.

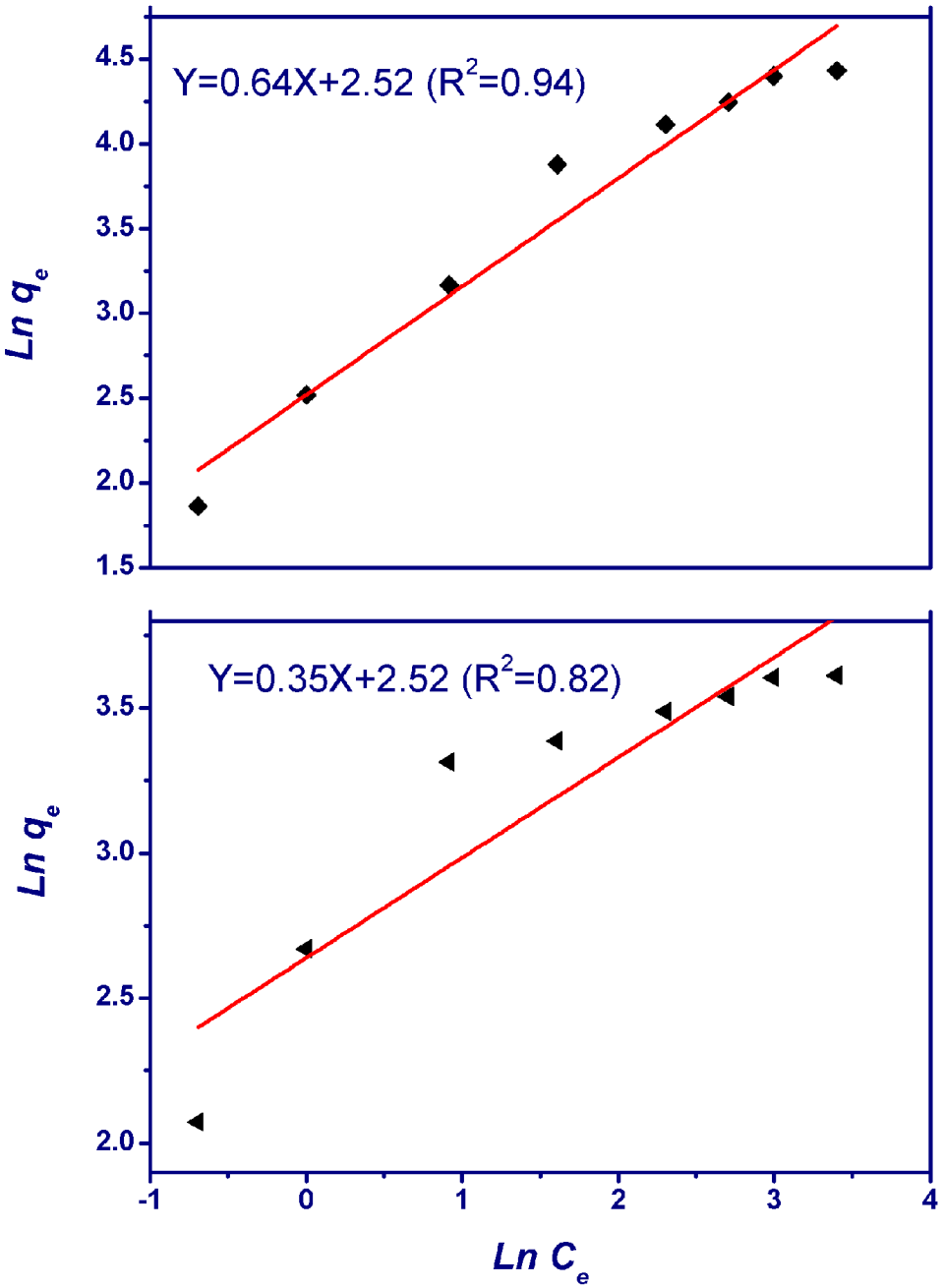

Figure S16. XPS survey spectra of the as-synthesized γ-Fe_2O_3 NSs before and after loaded with As(III)/As(V) at defferent condition. High As signal can be seen for all As(III) loaded sample. While for As(V) treated sample, good As(V) signal was only observed at pH 3.0 or in the presence of 200 mM NaCl.

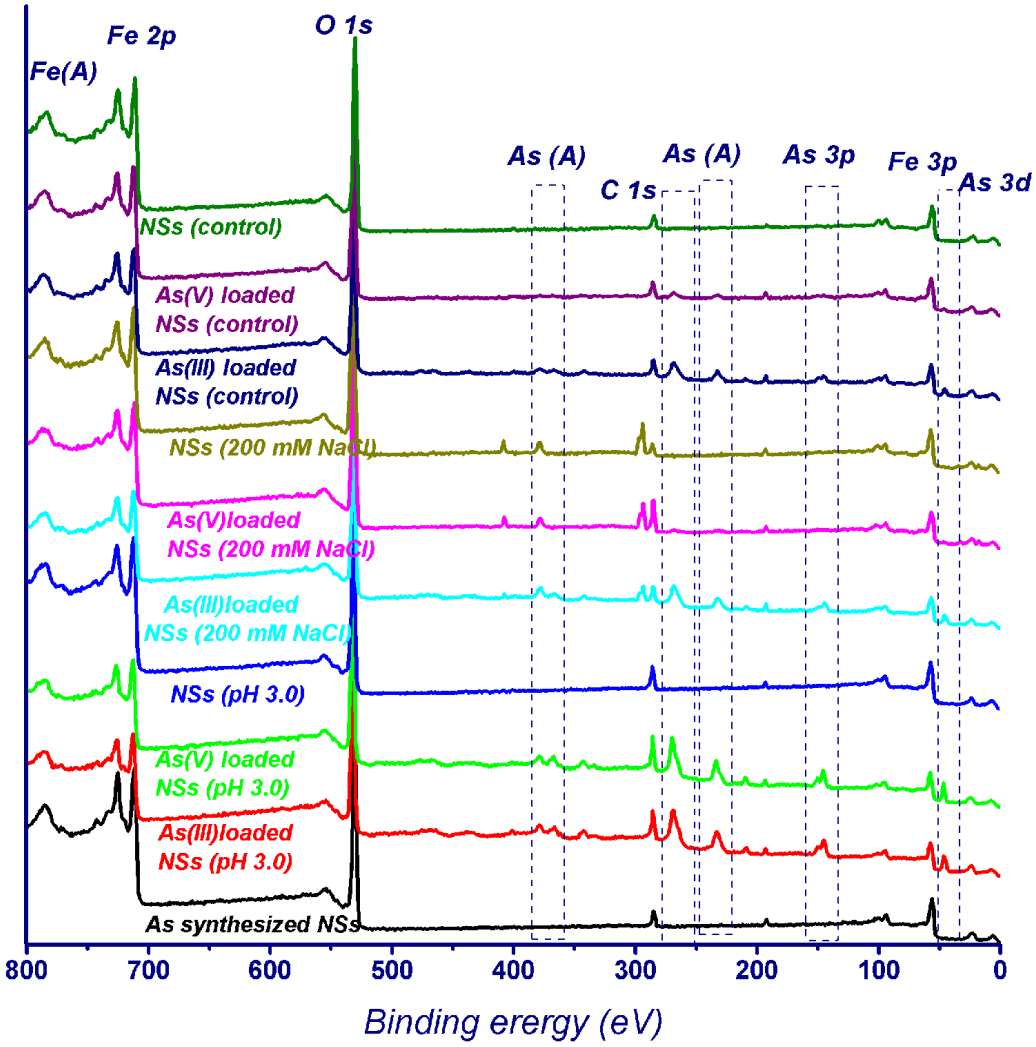

Figure S17. Different adsorption configuration of As ions on γ-Fe_2O_3 NSs surface and the alternation on surface –OH amount. Only the formation of linear monodentate complexion results in the net increase of surface –OH.

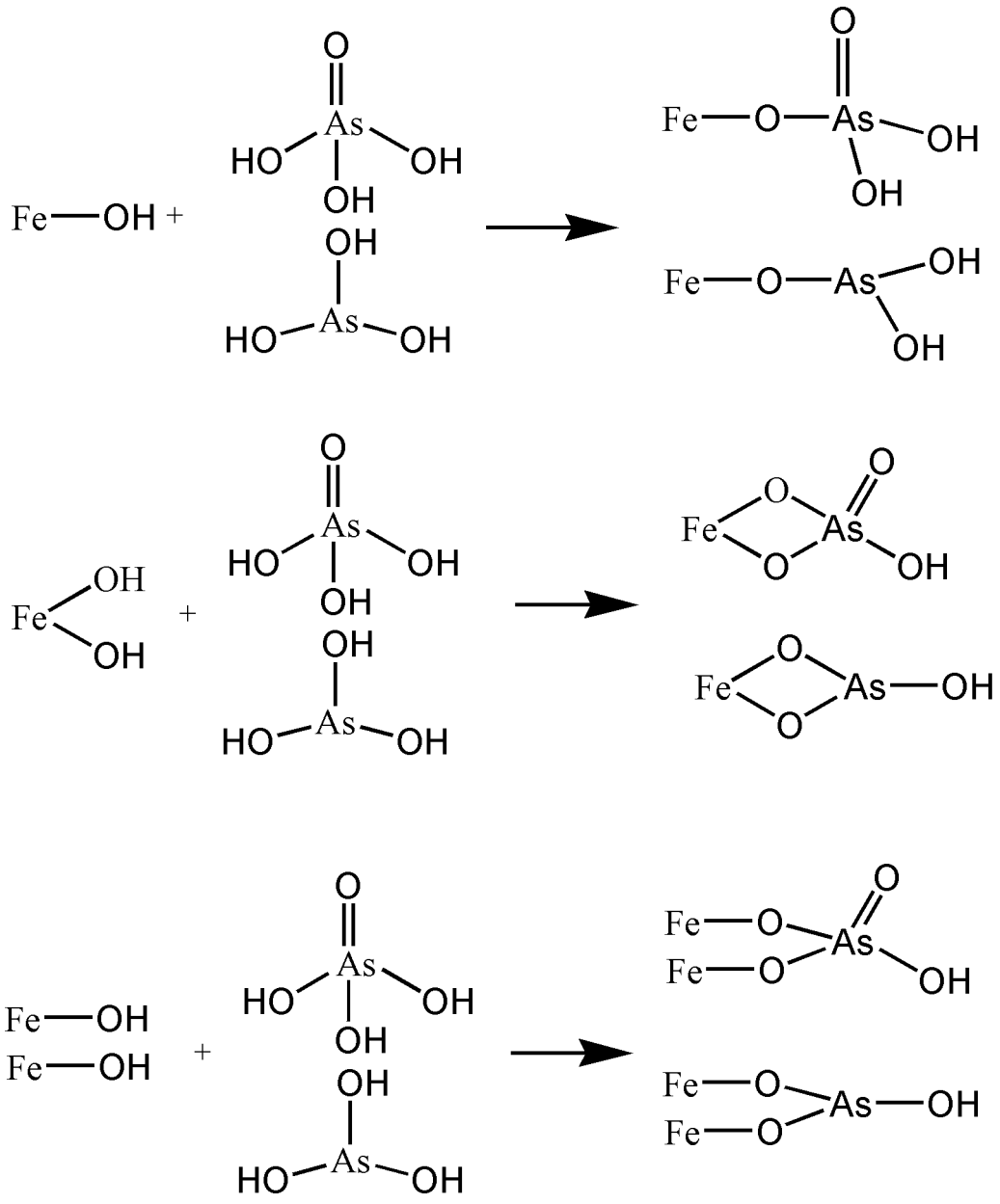

Figure S18. High-resolution O_{1s} XPS spectrum of the as-synthesized γ-Fe_2O_3 NSs. The surface –OH is as high as 40.58%, which is very important for the capture of As ions.

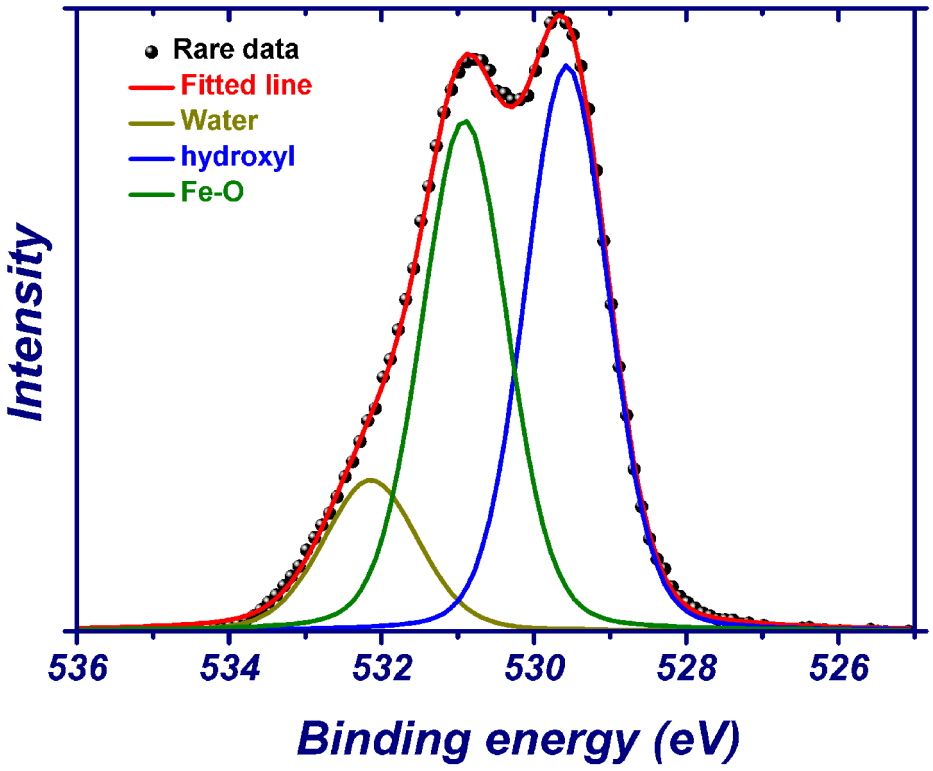

Figure S19. Regeneration the spent γ-Fe_2O_3 NSs sorbent with 10.0 mM NaOH, and the Arsenic ion adsorption performances of the regenerated NSs in the subsequent round of use.

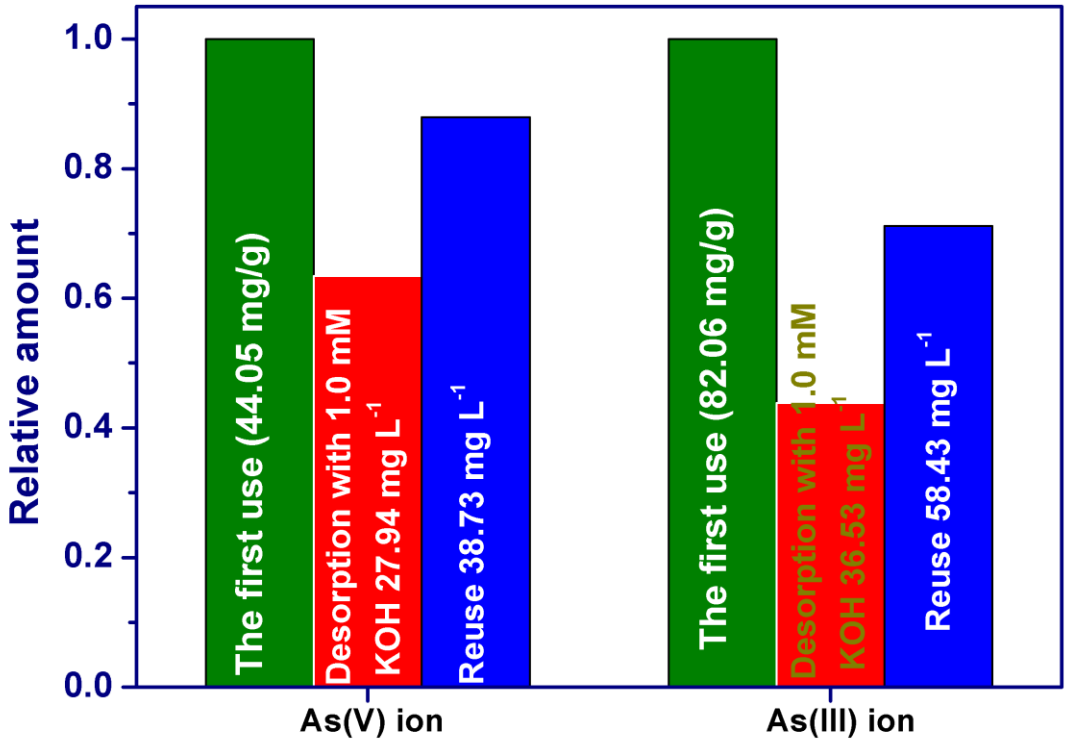

Figure 20. Arsenic solid stability analysis by the Toxicity Characteristic Leaching Procedure (TCLP), the concentration of Arsenic species in the solution leach by 50 g L^{-1} γ-Fe_2O_3 NSs that loaded with 82.06 and 44.05 mg g^{-1} As(III) and As(V) ion were monitored at the first, second, third, fifth and the tenth day.

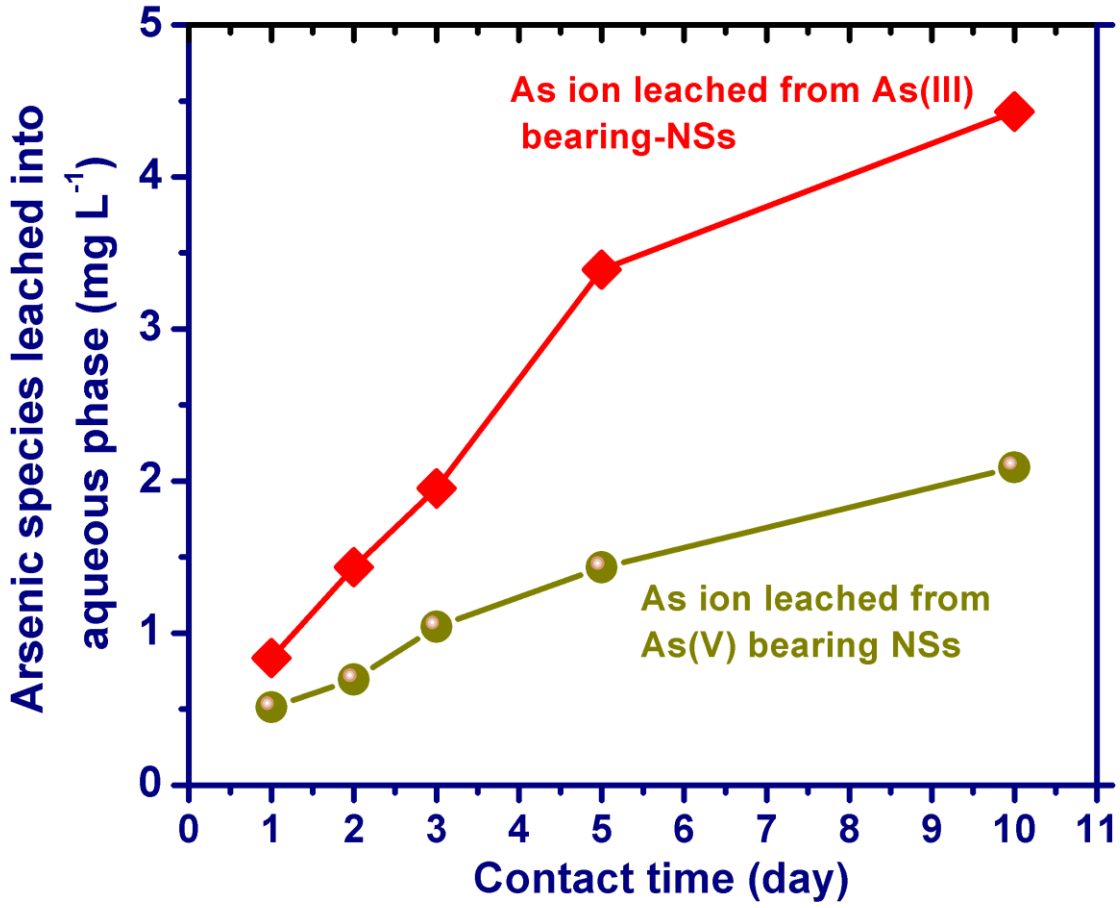

Table S1. The pseudosecond-order adsorption model fitting parameters of As(III) adsorption kinetics on 0.1 g L^{-1} γ-Fe_2O_3 NSs

Ce (mg L^{-1})	Calculated qe (mg.g^{-1})	k2(g.mg^{-1}.min^{-1})	R^2
0.5	5.22	0.0399	0.999
1.0	11.30	0.0285	1.000
2.5	23.72	0.0047	0.997
5.0	48.31	0.0030	0.999
10.0	61.16	0.0029	0.999
15.0	69.74	0.0027	0.999
20.0	81.37	0.0024	0.999
30.0	84.03	0.0016	0.999

Table S2. The pseudosecond-order adsorption model fitting parameters of As(V) adsorption kinetics on 0.1 g L^{-1} γ-Fe_2O_3 NSs.

Ce (mg L^{-1})	Calculated qe (mg.g^{-1})	k_2(g.mg^{-1}.min^{-1})	R^2
0.5	7.94	0.0233	0.999
1.0	14.43	0.0128	0.999
2.5	27.48	0.0067	0.999
5.0	29.61	0.0042	0.994
10.0	32.79	0.0040	0.998
15.0	34.63	0.0035	0.999
20.0	36.72	0.0029	0.994
30.0	37.05	0.0021	0.998

Table S3. The Languir and Freundlich model fitting parameters.

	Langmuir model			**Freundlich model**		
	a	**b**	**R^2**	**k**	**n**	**R^2**
As(III)	109.3	0.12	0.992	14.01	1.56	0.956
As(V)	39.1	0.60	0.998	12.15	2.89	0.824

Table S4. Fitted date for the high resolution O1s XPS spectra.

		Absorbed water		Surface hydroxyl		Lattice O		Increase in hydroxyl group
		B.E. (eV)	Amount	B.E.(eV)	Amount	B.E.(eV)	Amount	
Pristine	---	532.1	17.19%	530.95	40.58%	529.65	42.23%	-----
pH 3.0	As(III)	532.13	21.71%	530.84	46.58%	529.71	31.71%	89.30%
	As(V)	532.15	20.05%	530.89	49.39%	529.74	30.56%	100.00%
	Blank	532.14	17.89%	531.02	24.61%	529.81	57.51%	---
200 mM	As(III)	532.15	22.88%	530.82	43.26%	529.6	33.86%	23.21%
NaCl	As(V)	532.17	22.90%	530.81	41.60%	529.56	35.50%	18.49%
	Blank	532.25	25.07%	530.47	35.11%	529.67	39.82%	-----
Normal	As(III)	532.09	18.44%	530.83	44.14%	529.56	37.42%	7.88%
	As(V)	532.2	15.92%	530.89	42.47%	529.63	41.61%	3.78%
	Blank	532.2	14.25%	530.82	40.92%	529.47	44.83%	---

Table S5. Structure parameters derived from As K-edge EXAFS analysis.

shell	CN [a]	R (Å) [b]	σ^2 (Å^2) [c]	ΔE_0(eV)[d]	R-factor[e]
As-O	4.09	1.69 ±0.01	0.003 ±0.002	5.78	0.019
As-Fe	0.74	3.31 ±0.04	0.004±0.006		

[a] coordination number. [b] interatomic distance. [c] Debye-Waller factor. [d] threshold energy shift. [e] goodness-of-fit parameter: R-factor = $\Sigma(\chi_{data} - \chi_{fit})^2/\Sigma(\chi_{data})^2$

Table S6. Inorganic arsenic ion removal performance in natural water samples (10 mL) with the as-synthesized γ-Fe_2O_3 NSs (0.15 mgL^{-1})

Sample	Spiked (μg/L)	As(V) (μg/L) in water samples		As(III) (μg/L) in water samples	
		Before treatment	After treatment	Before treatment	After treatment
1	0	826.2	0.42	ND	ND
	500.0	1326.2	0.83	500.0	1.92
	1000.0	1826.3	4.90	1000.0	2.99
	2000.0	2826.2	5.62	2000.0	9.34
2	3000.0	3826.2	9.37	3000.0	18.13
	0	11.96	<0.10	ND	ND
	500	511.96	0.61	500.0	2.11
	1000	1011.96	1.32	1000.0	6.66
	2000	2011.96	4.34	2000.0	12.14
3	3000	3011.96	8.71	3000.0	32.17
	0	8.25	<0.10	ND	ND
	500	508.25	0.68	500.0	3.95
	1000	1008.25	1.54	1000.0	5.33
	2000	2008.25	5.45	2000.0	8.84
4	3000	3008.25	9.08	3000.0	17.45
	0	9.11	<0.10	ND	ND
	500	509.11	0.30	500.0	1.85
	1000	1009.11	0.99	1000.0	5.52
	2000	2009.11	2.50	2000.0	7.88
5	3000	3009.11	4.03	3000.0	32.23
	0	11.29	<0.10	ND	ND
	500	511.29	0.35	500.0	0.79
	1000	1011.29	0.39	1000.0	1.84
	2000	2011.29	1.2	2000.0	9.17
	3000	3011.29	3.31	3000.0	21.43

***Table S7*.** pH and the concentration of other ions in the tested water samples.

	Sample 1	**Sample 2**	**Sample 3**	**Sample 4**	**Sample 5**
pH	8.87	7.68	7.46	8.31	7.92
K[a]	1.48	2.14	10.47	3.18	0.81
Ca	21.12	66.83	69.86	27.65	66.54
Mg	22.59	14.68	17.63	28.63	26.28
Na	346.29	458.47	282.36	627.27	294.52
Fe	0.26	0.055	0.020	0.032	ND
Cu	1.16	0.53	0.26	0.57	0.21
Zn	0.55	0.29	0.21	0.16	0.17
Al	ND	ND	ND	0.04	ND
P	0.46	1.26	1.17	0.22	2.08
S	ND	25.37	10.88	29.70	11.85
Si	9.38	36.26	35.96	21.30	19.01

[a] all ions were determined by ICP-AES, and this technology is not sensitive to Br and Cl.